

Thermodynamic characterization of a macrocyclic Zika virus NS2B/NS3 protease inhibitor and its acyclic analogs

Stefan J. Hammerschmidt¹ | Simon Huber² | Niklas J. Braun² | Marc Lander¹ |
Torsten Steinmetzer² | Christian Kersten¹ 

¹Institute of Pharmaceutical and Biomedical Sciences, Johannes Gutenberg-University, Mainz, Germany

²Institute of Pharmaceutical Chemistry, Philipps-University, Marburg, Germany

Correspondence

Christian Kersten, Institute of Pharmaceutical and Biomedical Sciences, Johannes Gutenberg-University, Staudingerweg 5, 55128 Mainz, Germany.
Email: kerstec@uni-mainz.de

Funding information

LOEWE-Zentrum für Translationale Medizin und Pharmakologie, Grant/Award Number: DRUID (Novel Drug Targets against Poverty-Related; Deutsche Forschungsgemeinschaft, Grant/Award Number: INST 247/921-1 FUGG

Abstract

Cyclization of small molecules is a widely applied strategy in drug design for ligand optimization to improve affinity, as it eliminates the putative need for structural preorganization of the ligand before binding, or to improve pharmacokinetic properties. In this work, we provide a deeper insight into the binding thermodynamics of a macrocyclic Zika virus NS2B/NS3 protease inhibitor and its linear analogs. Characterization of the thermodynamic binding profiles by isothermal titration calorimetry experiments revealed an unfavorable entropy of the macrocycle compared to the open linear reference ligands. Molecular dynamic simulations and X-ray crystal structure analysis indicated only minor benefits from macrocyclization to fixate a favorable conformation, while linear ligands retained some flexibility even in the protein-bound complex structure, possibly explaining the initially surprising effect of a higher entropic penalty for the macrocyclic ligand.

KEYWORDS

crystallization, macrocycles, molecular dynamics, thermodynamics, Zika NS2B/NS3 protease

1 | INTRODUCTION

1.1 | Zika virus (ZIKV) infection

ZIKV infections gained worldwide interest since they became endemic in Brazil in 2015. In this outbreak, approximately 400,000 to 1.6 million people were infected. Besides the transmission via its main vectors *Aedes aegypti* and *Aedes albopictus*, whose occurrences are typically associated with flaviviral distribution, it was also discovered to be spread by sexual intercourse.^[1–5] A typical ZIKV infection is accompanied by mild flu-like symptoms and a high prevalence of asymptomatic cases. As a result of widespread ZIKV infection cases all over South America and its correlation to neurological disorders such as the Guillain–Barré syndrome and microcephaly in neonates, the WHO declared ZIKV a public health emergency in 2016.^[6–10]

1.2 | NS2B/NS3 protease

In the viral replication cycle, the viral genome is translated into a precursor-polyprotein processed by the viral NS2B/NS3 serine protease and host proteases into the three structural (Capsid, Membrane, and Envelope) and the seven nonstructural (NS) proteins (NS1, NS2A, NS2B, NS3, NS4A, NS4B, and NS5).^[11] When this crucial function of NS2B/NS3 is inhibited, viral replication is abolished. Therefore, the NS2B/NS3 protease resembles an attractive drug target to counter ZIKV infections.^[12–15] For the proteolytic activity of flaviviral proteases, the NS3 protease domain relies on its NS2B cofactor, which can adopt at least two conformations. In the inactive and so-called *open* conformation, NS2B is loosely bound to the NS3 protease domain and mainly disordered.^[16,17] In the catalytically active *closed* conformation, NS2B is wrapped around NS3 and contributes to substrate recognition by forming

This is an open access article under the terms of the Creative Commons Attribution License, which permits use, distribution and reproduction in any medium, provided the original work is properly cited.

© 2022 The Authors. *Archiv der Pharmazie* published by Wiley-VCH GmbH on behalf of Deutsche Pharmazeutische Gesellschaft.

parts of the S2 and S3 binding pockets.^[18–20] In solution, both conformations coexist in equilibrium.^[21–23] Upon ligand or substrate binding to the active site, exclusively cocrystals of the closed conformation were obtained so far.

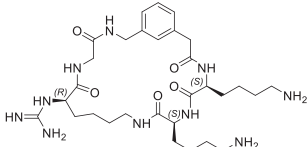
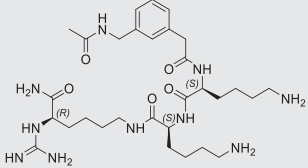
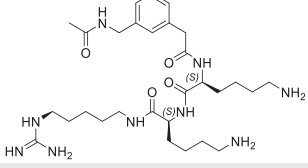
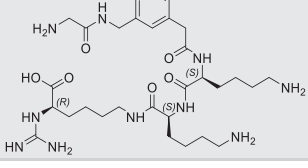
1.3 | Inhibitor design and optimization

Due to the shallow shape of the NS2B/NS3 active site^[24] and its preference for basic P1 and P2 residues, the development of drug candidates targeting this site is considered to be very challenging.^[25] Consequently, most active site-directed ZIKV NS2B/NS3 protease inhibitors are based on peptidic or peptidomimetic scaffolds with often limited bioavailability featuring multibasic scaffolds.^[12,26–29] Although they reached considerably high affinities, these compounds exhibited only poor antiviral potency most likely caused by limited membrane permeabilities.^[30–33] The crystal structure of a linear substrate analog inhibitor in complex with the closely related West Nile virus NS2B/NS3 protease revealed a horseshoe-like backbone conformation with both termini in close proximity to each other (Protein Data Bank^[34] [PDB]-ID: 2YOL; Supporting Information: Figure S1).^[35] This gave rise to a macrocyclization approach not only intended to optimize the inhibitory potency but also increase membrane permeability resulting in compound **1** (Table 1).^[27] In the cocrystal structure of inhibitor **1** in complex with ZIKV NS2B/NS3 (PDB-ID: 6Y3B, Figure 1), the P1 guanidine residue is located at the bottom of the S1 pocket and forms an ionic interaction with Asp129. The carbonyl oxygen of Gly159 forms a hydrogen bond directly to the guanidine as well as a water-mediated

hydrogen bond. Other H₂O-mediated interactions are formed by Asp129 to the backbone nitrogen of the glycine linker. An intramolecular interaction between the P4 carbonyl oxygen and the terminal guanidine nitrogen stabilizes the inhibitor's conformation. This interaction can also be found in the linear reference inhibitor (Supporting Information: Figure S1). The hydroxy group of Tyr161 stabilizes the position of the backbone of inhibitor **1** by forming hydrogen bonds between its hydroxy group to the nitrogen of the P1–P2 amide and the backbone carbonyl oxygen of P3 Lys that further interacts with the Gly153 nitrogen. The side chain of the P2 Lys forms polar contacts to the NS2B Asp83 and NS3 Asn152 side chains and to the Gly82 backbone in the S2 pocket. The side chain of P3 Lys is stabilized by polar interactions with the carbonyl oxygen of Phe84 and the S3 forming side chains of Asp83 and Ser85. It is noteworthy that the NS2B residues Asp83 and Ser85 are found in two conformations based on their occupancies in the crystal structure. Therefore, Asp83 can contribute to the stabilization of both the P2 Lys and the P3 Lys side chain.

The complex formation of an oligo-peptidic ligand with a protein is often accompanied by the fixation of rotatable bonds upon binding.^[18] This reduction of conformational degrees of freedom is usually accompanied by an entropic penalty and, thus, lowers binding affinity. In ligand optimization attempts, a widely accepted strategy to increase affinity is the rigidification of rotatable bonds to preorganize the ligand in the binding conformation via (macro-) cyclization.^[18,36] Although it is tempting to assume that mainly entropic effects lead to affinity enhancement by cyclization, also enthalpic benefits have been reported, which has led to some controversy about the underlying physical principles.^[37–40] In the case of peptidomimetics, macrocyclization,

TABLE 1 Affinity and buffer-corrected thermodynamic binding profiles obtained by the fluorometric enzyme activity assay and ITC

Compound	Structure	K _i (nM)	K _d (nM)	ΔG° (kJ·mol ⁻¹)	ΔH° (kJ·mol ⁻¹)	-TΔS° (kJ·mol ⁻¹)	n _{proton}	ΔC _p (kJ·mol ⁻¹)
1		1.24 ± 0.08	110 ± 7	-40.1 ± 1.7	-74.8	34.7	0.17	-3.77
2		9.30 ± 0.72	2120 ± 440	-32.7 ± 0.3	-53.1	20.4	0.30	-2.16
3		99.7 ± 7.4	2700 ± 90	-31.9 ± 0.2	-58.5	26.6	-0.10	-2.90
4		384 ± 42	8220 ± 250	-29.5 ± 0.1	-77.3	47.8	0.24	N.d.

Abbreviations: ITC, isothermal titration calorimetry; N.d., not determined.

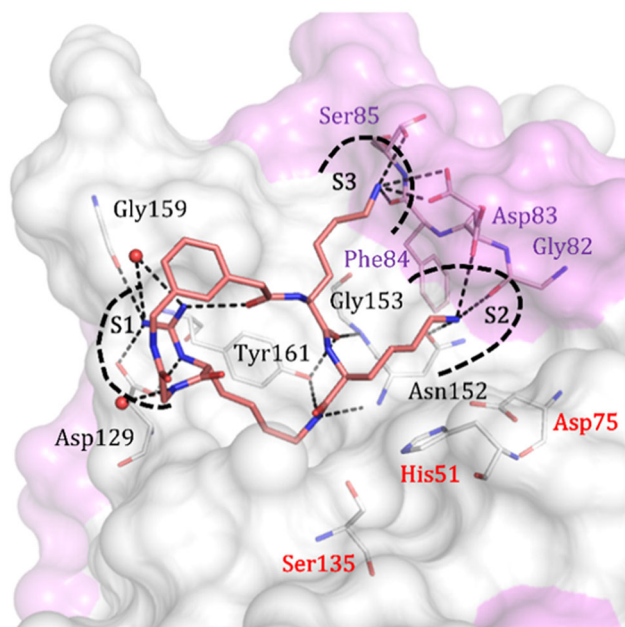


FIGURE 1 Binding mode of compound **1** in complex with the ZIKV NS2B/NS3 protease (PDB-ID: 6Y3B). Inhibitor **1** is depicted as sticks with salmon-colored carbon atoms. For a clear view, only amino acids forming polar interactions (black dashed lines) are shown as lines with violet (NS2B) and white carbon atoms (NS3). Amino acids forming the catalytic triad are labeled in red.

bridging, and cross-linking represent promising strategies to achieve more potent ligands with several benefits.^[27,41,42] Besides higher proteolytic stability,^[28] properly restrained molecules are less likely to adopt conformations to fit the binding pockets of off-target proteins; thus, macrocyclization offers a route to achieve more selective compounds.^[43] Additionally, by derivatization of polar terminal groups and reduction of the number of rotatable bonds, macrocyclization offers a convincing benefit to membrane permeability.^[29,30,44,45] Although the preorganization of ligands is a regularly utilized technique, the driving forces behind the improved affinities remain largely elusive. In rational drug design campaigns, isothermal titration calorimetry (ITC) is an indispensable tool to characterize binding thermodynamics. It allows to quantify the enthalpic (ΔH) and entropic ($-T\Delta S$) contributions to the overall binding free energy (ΔG) and to evaluate the impact of structural modifications on these parameters.

In this work, the thermodynamic effects of macrocyclization in inhibitor **1** compared to its noncyclic analogs **2–4** (Table 1) were investigated using a fluorometric enzyme activity assay, ITC, molecular dynamic (MD) simulations, and X-ray crystallography.

2 | RESULTS AND DISCUSSION

2.1 | Inhibitory activities

A fluorometric enzyme inhibition assay was employed to redetermine the inhibitory potencies of the compounds under elucidation. The obtained K_i values are in good agreement with

previous results^[26,27]: **1**: 1.24 ± 0.08 nM, **2**: 9.30 ± 0.72 nM; **3**: 99.7 ± 7.4 nM; and **4**: 384 ± 42 nM (Table 1).

2.2 | Thermodynamic binding profiles

In ITC experiments, the same affinity trend was observed but with significantly higher K_d values compared to K_i (Table 1), as occasionally observed when comparing different techniques.^[46,47] Interestingly, there are large differences in the factors between K_i and K_d (ca. 87 for inhibitor **1**, 228 for inhibitor **2**, 27 for inhibitor **3**, and 21 for inhibitor **4**; Table 1). The main differences in the experimental composition between the inhibition assay and ITC binding assay are the different concentrations of enzymes and ligands (Assay: 2 nM NS2B/NS3; ITC: 15–40 μ M NS2B/NS3) and the presence of a substrate in the inhibition assay and its absence in the ITC assay. One could speculate that the conformational equilibrium between inactive open conformation and active closed conformation of the protease is affected by the substrate's presence. As the inhibitors under elucidation also bind to the active closed conformation, a shift of equilibrium by the substrate to this conformation might enhance the effective inhibitory potency.^[46,47] However, this hypothesis requires further elucidation and is beyond the scope of this manuscript. The buffer-corrected thermodynamic binding profiles (Table 1, buffer correction calculation and signature plots: Supporting Information: Figure S2, measurements in different buffers: Supporting Information: Table S1) revealed that the affinity of all tested inhibitors is driven by their large exothermic binding enthalpy with the highest contribution for inhibitors **1** and **4** ($\Delta H^\circ = -74.8$ and -77.3 kJ \cdot mol $^{-1}$) and lower binding enthalpies for inhibitors **2** and **3** ($\Delta H^\circ = -53.1$ and -58.5 kJ \cdot mol $^{-1}$). Furthermore, all inhibitors show a positive temperature-dependent entropy term ($-T\Delta S^\circ$). Again, the macrocyclic compound **1** and linear compound **4** share higher absolute values ($-T\Delta S^\circ = 34.7$ and 47.8 kJ \cdot mol $^{-1}$, respectively) than inhibitors **2** and **3** ($-T\Delta S^\circ = 20.4$ and 26.6 kJ \cdot mol $^{-1}$). Consequently, the increased affinity of inhibitor **1** compared to **2** and **3** is despite the macrocyclization not being accompanied by a favorable entropy term. Similar results of macrocyclization were reported in the literature.^[37,40] Buffer ionization correction also revealed that probably no proton transfers occur for all inhibitors **1–4** upon complex formation ($n_{\text{proton}} = 0.17, 0.30, -0.10,$ and 0.24 , respectively, Table 1, Supporting Information: Figure S2). Inhibitors **1–3** share three basic centers: the guanidinium moiety and the aliphatic amines of the lysine sidechains. All of these tend to be protonated under physiological pH and this protonation seems not to change upon binding as all three moieties are involved in polar, ionic interactions (Figure 1). Inhibitor **4** contains two additional functionalities, a basic amine, and an acid. Again, binding seems not to change protonation states. In solution as well as within the complex, all mentioned moieties should be charged. Finally, isobaric heat capacity changes (ΔC_p) were determined from ITC experiments at different temperatures (Supporting Information: Table S2). Changes in heat capacity are commonly correlated with the burial of nonpolar and polar surfaces indicating desolvation

effects.^[48,49] For inhibitors 1–3, negative ΔC_p -values of -3.77 , -2.16 , and -2.88 $\text{kJ}\cdot\text{mol}^{-1}\cdot\text{K}^{-1}$ were determined (Supporting Information: Figure S3). Differently, for compound 4, no linear correlation between ΔH and temperature was observed. While the negative ΔC_p -values of 1–3 indicate the burial of hydrophobic areas, the absolute values are very large for pure protein–ligand interactions.^[50–52] Most likely, the shifted equilibrium between open and closed conformations upon active site-directed ligand binding is also accompanied by burial of hydrophobic areas. This is also suggested by a decrease in the fraction of hydrophobic accessible surface area from 52% in the open to 48% in the closed ZIKV NS2B/NS3 conformation and seems to be a common feature for flaviviral proteases (Supporting Information: Table S3). In the closed (active) conformation, the NS2B cofactor is tightly wrapped around NS3 while being more solvent exposed in the open conformation. Hence, the largest ΔC_p of compound 1 compared to 2 and 3 could be interpreted in different ways, like the stronger burial of hydrophobic patches of the ligand or a more efficient shift of the conformational equilibrium toward the closed conformation. However, ITC alone cannot finally answer that question and several layered effects may contribute to the observed results.^[53–55]

2.3 | Molecular dynamics

To further elucidate this binding behavior, molecular dynamic simulations (MDs) were conducted starting from the ZIKV NS2B/NS3-1 complex structure (PDB-ID 6Y3B).^[27] For inhibitors 2–4, starting from the same structure, ligands were modified and energetically minimized within the binding site prior to MD as at that time no complex structures of NS2B/NS3 with those ligands were available in the PDB. Throughout the simulations of the NS2B/NS3–inhibitor complexes, it was observed that inhibitors 2 and 3 retained some partial flexibility even in the protease-bound state, while the macrocycle 1 and inhibitor 4 (4 likely due to an intramolecular ionic interaction between the charged termini) are highly rigid (Figure 2a). For inhibitors 2 and 3, the acetylated 3-aminomethylphenylacetyl group was found to be more flexible in the bound state, whereas the P2 and P3 Lys sidechains stayed in a stable orientation. Tracking the rigid and flexible parts of the ligands over the MD trajectory (Figure 2b), for inhibitors 1 and 4, both RMSD traces (rigid part only and whole molecule) stayed below 2.2 Å over 10 ns of simulation time, whereas the RMSD at the flexible parts of compounds 2 and 3 drastically increases throughout the simulation compared to the RMSD only of the rigid parts. To further elucidate the ligand flexibility based on MD, the internal torsion energies of the bound and unbound states were investigated. In analogy to the SPAM method,^[56] which is used to estimate binding thermodynamics of water molecules from MD simulations, the distributions of ligand torsion energies were computed (Figure 2c). One should be aware that the transfer of this method from water to a more complex system neglects many parts of molecular recognition and might not be used as a

quantitative metric. For a qualitative interpretation of torsion energy distribution and its implications on ligand flexibility, however, it might give insight into torsional degrees of freedom and their changes upon binding. In our variant of this method, the energies of all torsion angles are calculated throughout the simulations of ligands in the bound and unbound state. The torsion energies were found to follow a Gaussian distribution for all ligands, which is also found for the interaction energies of water molecules in the original SPAM method. This normal distribution is a prerequisite for further elucidation. The difference in the mean value of torsion energies between bound and unbound ligands indicates how favorable the bound conformation is in terms of torsion strain. A shift to higher values indicates that the bound conformation might be less favorable than other conformations found in the solution. The broadness of the distribution (indicated by the standard deviation of the Gaussian fitting curve) might be a surrogate for the degrees of torsional freedom in bound and unbound states and subsequently on its changes upon binding. A sharper distribution of ligand torsion energies in the bound state compared to the free ligand could indicate rigidification upon complex formation. This was observed for both inhibitors 1 and 4, but for compounds 2 and 3, no such pronounced effect was noticed with a similarly sharp distribution of torsion energies in the bound and unbound state. This observation might indicate one reason for the more favorable temperature-dependent entropy term ($-T\Delta S^\circ$) of inhibitors 2 and 3, which retain more torsional degrees of freedom in the complex with ZIKV NS2B/NS3 compared to inhibitors 1 and 4. Further, for compound 1, the highest shift of the average torsion energy toward higher values was observed, indicating that the conformation trapped by macrocyclization might not be optimal and structural reorganization is still required upon binding.

Notably, changes in the conformational entropy of the protein could easily dominate binding entropies. Interestingly, while some rigidification of NS2B/NS3 upon ligand binding was observed when comparing apo- and ligand-bound structures, especially within the binding site, there were no obvious differences observed between the ligands. Both structural changes (indicated by residual C_α -RMSD) and backbone dynamics (C_α -root-mean-square fluctuation, RMSF) in complex with the different ligands were broadly similar (Supporting Information: Table S4, Figure S4a,b). Subsequently, order parameters (S^2) for both backbone and sidechains were investigated (Supporting Information: Table S5, Figure S4c,d). S^2 are associated with the conformational entropy of residues^[57] with $S^2 = 1$ indicating low flexibility and $S^2 = 0$ indicating high flexibility.^[58,59] Backbone S^2 are fairly in line with the RMSF with only Gly159 and Ser160 being a little more flexible in the NS2B/NS3-2 complex. Sidechain S^2 showed overall more differences but no obvious trends that discriminate inhibitors 1 and 4 binding from inhibitors 2 and 3. However, even though differences in S^2 for certain residues both within the binding site and more distant were observed, the corresponding configurational entropies of the residues seem to approximately cancel each other out. Therefore, the analysis of protein residue dynamics remains inconclusive, but slight differences might not hold the explanation for the observed thermodynamic binding profiles from the ITC experiments.

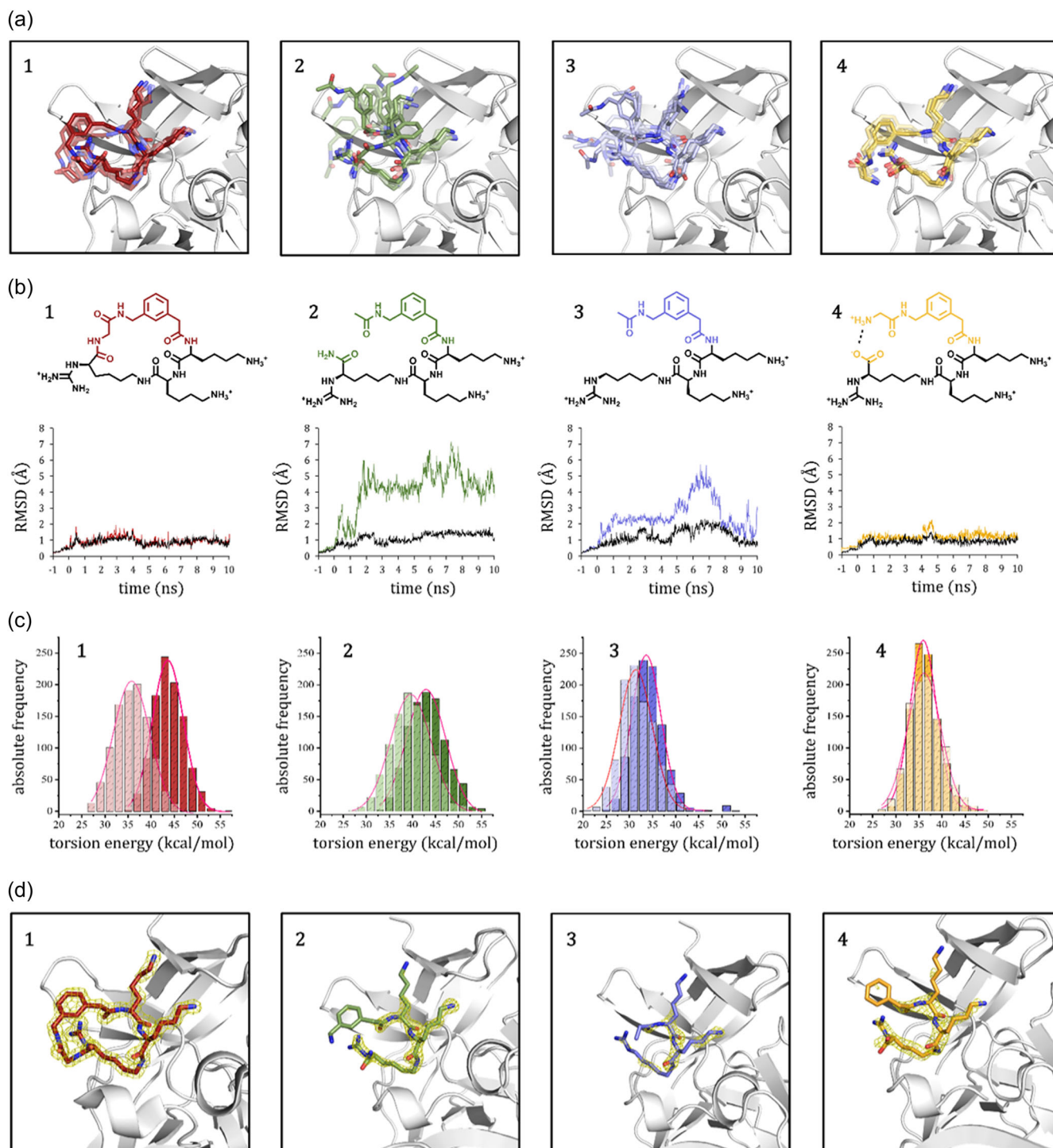


FIGURE 2 Investigating ligand flexibilities of 1 (red), 2 (green), 3 (blue), and 4 (yellow) in complex with NS2B/NS3 (white). (a) Ligand overlay of six MD frames (after 0, 2, 4, 6, 8, and 10 ns). The transparency reduces with elapsed time. For a clear view, only the starting structure of the enzyme is shown. (b) 2D structures of inhibitors 1-4 (top) and heavy atom root mean square deviation (RMSD) traces over 10 ns simulation time (bottom). The flexible parts of inhibitors 2 and 3 and corresponding atoms of inhibitors 1 and 4 are colored. RMSD traces are shown for the entire molecule (colored) and the more rigid part only (black). (c) Calculated ligand torsion energy distributions in the unbound (transparent) and the complexed (opaque) state. (d) Crystallographic binding modes of all inhibitors 1-4 in complex with ZIKV NS2B/NS3 (PDB-IDs: 6Y3B, 7ZLD, 7ZLC, and 7ZMI) with the $2F_o - F_c$ simulated annealing omit maps (yellow) are shown at $\sigma = 2.0$ for inhibitors 1 and 2, $\sigma = 1.5$ for inhibitor 3, and $\sigma = 1.0$ for inhibitor 4.

2.4 | X-ray crystallography

These findings were further supported by crystal structure analysis. By the time, co-crystal structures of inhibitors 2–4 in complex with NS2B/NS3 could be obtained (Supporting Information: Table S6). All ligands revealed a highly similar binding mode in line with the starting structures from MD simulations. Intriguingly, lower electron densities were observed for the ligand atoms, which should remain highly flexible according to the MDs (Figure 2d). This was true when investigating the simulated annealing omit maps at $\sigma=2$ for compounds 1 and 2 and $\sigma=1.5$ for compound 3. For the low-affinity ligand 4, however, the map is shown for $\sigma=1$. This compound is only resolved poorly, possibly due to its lower overall binding affinity and the lower crystal structure resolution (Supporting Information: Table S6). However, this torsion-centric interpretation neglects the manifold other effects of ligand binding on the thermodynamic binding profiles. Especially desolvation effects and target rigidification may have a strong impact on entropy as well. The binding modes are highly conserved between the different ligands resembling the observed interactions of the NS2B/NS3-1 complex (Figures 1 and 2d). The low electron density of the *N*-terminal amide of inhibitors 2 and 3 and the aromatic system of 3 indicates the flexibility of these moieties. Notably, rather than being involved in direct protein–ligand interactions, these parts are oriented toward the solvent and “hovering above” the guanidinium group of the ligands (Figure 3). On the one hand, this can stabilize the ligand's binding

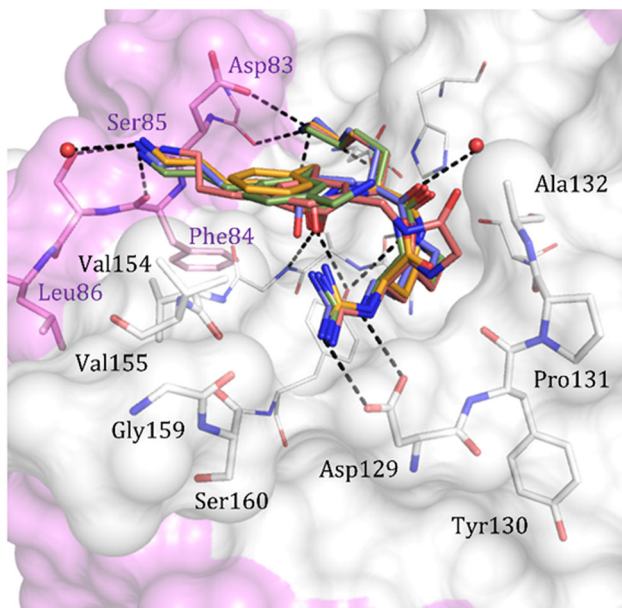


FIGURE 3 Overlay of binding modes of compounds 1–4 in complex with the ZIKV NS2B (magenta)/NS3 (white) protease (PDB-IDs: 6Y3B, 7ZLD, 7ZLC, and 7ZMI). Inhibitors are depicted as sticks with colored carbon atoms (1: salmon, 2: green, 3: blue, 4: yellow). Polar interactions are shown as black dashed lines. For a clear view, only residues from the NS2B/NS3-3 complex are shown and only those residues with differences in B' -factors depending on which ligand is bound (as described in the main text) are labeled.

mode via intramolecular cation– π interaction. On the other hand, the higher flexibility of that moiety can also indicate its reduced desolvation as hinted by the lower absolute ΔC_p -values of 2 and 3 compared to 1 (Table 1). Finally, 4 is the only ligand containing an acidic, negatively charged moiety reducing its potency as the active site has a highly negative potential (Supporting Information: Figure S5). Furthermore, strong interactions often result in a loss of conformational degrees of freedom for both ligands and proteins and subsequently are accompanied by an enthalpy–entropy compensation.^[53,60] Therefore, B-factors as a surrogate for residue flexibility of the NS2B/NS3–inhibitor complexes were further analyzed. While raw B-factors are highly influenced by resolution, crystal packing, or refinement methods used, B-factors were normalized with the BANΔIT webserver for comparability between the different structures.^[16] This analysis of normalized B' -factors indicated that some binding site residues in the complexes with inhibitors 2–4 retain higher flexibility (high B' -factors) while binding-site residues are slightly more rigid (lower B' -factor) for the NS2B/NS3-1 complex. This holds true in general, but especially for NS3 residues 129–132 and Gly159 (S1 pocket), Val154, Val155, Ser160, and Tyr161 (close to the aromatic linker) and residues 83–86 of the S3 pocket formed by NS2B (Figure 3, Supporting Information: Figure S4E, Supporting Information: Table S7). All these residues are located around the termini of the acyclic ligands and the linking position of macrocycle 1. Hence, the tight binding of inhibitor 1 might also result in a rigidification of the protein and subsequently an accompanied entropic penalty. While protein dynamics can be influenced by ligand binding in regions distant from the binding site, B' -factors showed some minor differences there as well. However, residues with the highest B' -differences are primarily located at the termini or in loop regions where flexibility is usually higher and larger deviations between different structures are observed regularly (e.g., NS2B residues 64–68 and NS3 residues 29–32, Supporting Information: Figure S4e).^[16] Therefore, it can be presumed that the highly similar binding modes of 1–4 result in similar global effects for protein dynamics.

3 | CONCLUSION

Cyclization and macrocyclization are common strategies in drug design and optimization. One key aspect is the generally accepted hypothesis that cyclic ligands trapped in the bioactive conformation require less structural preorganization and rigidification upon binding and hence are accompanied by a lower entropic penalty. The protonation-corrected thermodynamic binding profiles from ITC experiments of inhibitors 1–4 binding to the ZIKV NS2B/NS3 protease (Table 1, Supporting Information: Figure S2) revealed that this common explanation for the higher affinity of a macrocyclic compound was not valid for inhibitor 1 in comparison to inhibitors 2 and 3 and that the higher affinity of inhibitor 1 cannot be attributed to a beneficial $-T\Delta S^\circ$ term. Both inhibitors 1 and 4 have a higher temperature-dependent binding entropy of 34.9 and 47.8 $\text{kJ}\cdot\text{mol}^{-1}$, whereas the linear compounds 2 and 3 share a less

disturbing $-T\Delta S^\circ$ of 20.4 and 26.6 kJ·mol⁻¹, respectively. To further investigate these counterintuitive results, MD simulations and co-crystallization experiments were performed. The ligand RMSD traces and the torsion energy distributions derived from MD simulations indicated that inhibitors **2** and **3** retain some flexibility upon binding, whereas inhibitors **1** and **4** experience stronger rigidification upon complex formation. This observation was further supported by the crystallographically determined NS2B/NS3 complex structures of inhibitors **2–4**. Ligands **2** and **3** retain some flexibility in the complex as indicated by a lower electron density for the same atoms that appeared to be more flexible in the MDs. B'-factor analysis revealed that besides the ligand, also the protease binding site in the complex with macrocyclic ligand **1** is more rigid. While this ligand has a high binding enthalpy of $\Delta H^\circ = -75.1$ kJ·mol⁻¹, the accompanied entropic penalty is rather large with $-T\Delta S^\circ = 34.9$ kJ·mol⁻¹. As a word of caution, the thermodynamics of small molecules binding to proteins is way more complex and this torsion-centric evaluation neglects many additional underlying effects including slight differences in direct interactions and (de-) solvation. Additionally, large changes in heat capacity indicated that the observed effects might be shadowed by a conformational change as commonly described for the NS2B/NS3 protease. Hence, the interpretation is limited by the assumption that the high structural similarity within the described ligands results in similar direct protein–ligand interactions (Figures 2d and 3) and an equal effect on the conformational equilibrium. Subsequently, the study highlights the limitations in our understanding of how to link binding thermodynamics to structural features even for well-described systems covering ITC, crystallographic, and MD information. The interpretation can only describe a qualitative torsion effect rather than yielding quantitative energy terms to be directly correlated with ITC results. Nevertheless, the study demonstrates the possibilities of MD simulations in combination with structural biology to support the explanation of thermodynamic binding profiles for macrocycles. The implementation of additional model systems to identify common features of cyclic and acyclic ligand pairs might hold the potential to assist decision-making in prospective macrocycle design in the future.

4 | EXPERIMENTAL

4.1 | Chemistry

4.1.1 | Reagents

All reagents and solvents were purchased from Sigma-Aldrich Chemie GmbH, Thermo Fisher Scientific Inc., and Carl Roth GmbH + Co. KG.

4.1.2 | Synthesis

The synthesis and analytical characterization of inhibitors **1–4** and the substrate PhAc-LKKR-AMC are described in previous publications.^[27,35] The InChI codes of inhibitors **1–4**, together with some biological activity data, are provided as the Supporting Information.

4.2 | Recombinant protein expression and purification

The bivalently expressed ZIKV protease construct NS2B/NS3 (bZiPro) for enzyme inhibition assays and ITC experiments was expressed and purified, as described previously.^[26,61] Briefly, the vector (pETDuet) containing bZiPro (#86846, www.addgene.com) was transformed into competent *Escherichia coli* BL21 Gold (DE3) cells (Agilent Technologies) and grown in the LB medium containing 100 mg·L⁻¹ ampicillin at 37°C until an optical density (OD₆₀₀) of 0.8 was reached. Overexpression was induced overnight by the addition of 1 mM isopropyl- β -D-thiogalactoside (IPTG) at 18°C for 20 h. After harvesting by centrifugation at 9000 rpm at 4°C for 15 min, cells were flash-frozen in liquid nitrogen and stored at -80°C until further use. For purification of NS2B/NS3, the cell pellet was resuspended in buffer A1 (20 mM Tris-HCl pH 8, 300 mM NaCl, 20 mM imidazole, 0.1% (v/v) Triton_{X-100}, RNase, DNase, lysozyme, 1 mM DTT) and lysed by sonication (Sonoplus HD 2200). The lysate was cleared by centrifugation (20,000 rpm at 4°C for 1 h). The supernatant was subjected to immobilized metal affinity chromatography (IMAC) on a HisTrap HP 5 ml column (Cytiva Europe GmbH). After washing with buffer B1 (20 mM Tris-HCl, pH 8, 300 mM NaCl, 20 mM imidazole), the protein was eluted in a linear gradient to 250 mM imidazole. The His₆-tag was removed by thrombin protease cleavage during a dialysis step against buffer C1 (20 mM Tris-HCl, pH 8, 150 mM NaCl) overnight (4°C). After reverse IMAC to remove the His₆-tagged thrombin protease (kindly provided by Prof. Dr. Ute Hellmich, Institute of Organic Chemistry & Macromolecular Chemistry, Friedrich Schiller University Jena), NS2B/NS3 was further purified using a size exclusion chromatography step with a HiLoad 16/600 Superdex 75 column (GE Healthcare) in buffer C1. Collected fractions containing NS2B/NS3 were concentrated using Vivaspin 10 MWCO spin concentrators (Sartorius AG), flash-frozen in liquid nitrogen, and stored at -80°C. Protein identity and purity were confirmed by SDS-PAGE with Coomassie blue staining.

bZiPro for crystallographic experiments was expressed and purified in a similar manner with minor differences: Cell pellets were lysed with buffer A2 (20 mM sodium phosphate, pH 8.0, 500 mM NaCl, 2 mM β -mercaptoethanol, 10 mM imidazole, and 5% (v/v) glycerol). Nickel nitrilotriacetic acid (Ni-NTA) chromatography was performed using a HisTrap FF crude column (Cytiva Europe GmbH). After washing with buffer containing 20–30 mM imidazole, the protein was eluted with buffer B2 containing 150 mM imidazole. The His₆-tag was removed by the addition of thrombin, followed by dialysis of the mixture against buffer C2 (20 mM Na-HEPES, pH 7.5, 150 mM NaCl, 5% [v/v] glycerol, and 2 mM dithiothreitol [DTT]) for 20 h. After dialysis, the protein was further purified by size-exclusion chromatography using a HiLoad 26/600 Superdex 200 pg column (GE Healthcare).

4.3 | Enzyme inhibition assay

Fluorometric enzyme activity assays were performed on a Spark[®] (Tecan) microplate reader using white flat-bottom 96-well

microtiter plates (Greiner Bio-One). The substrate PhAc-Leu-Lys-Lys-Arg-7-amido-4-methylcoumarin (PhAc-LKKR-AMC) resembles the preferred cleavage site and releases fluorogenic AMC after cleavage. Assay buffer (180 μ l, 20 mM TRIS [pH 8.5], 10% [v/v] Glycerol, 0.01% [v/v] Triton_{X-100}, 2 mM DTT) was supplemented with 10 μ l of aqueous inhibitor solution in a half logarithmic dilution series (final concentrations ranging from $>25 \cdot IC_{50}$ to $<0.35 \cdot IC_{50}$) and 5 μ l of NS2B/NS3 to give a final protein concentration of 2 nM. The reaction was started by the addition of 5 μ l of substrate solution resulting in a 10 μ M final concentration. Fluorescence was monitored for 10 min at 25°C with excitation at 380 nm and detection at 460 nm. For the determination of the substrate K_M -value, 10 μ l of H₂O instead of the inhibitor solution was added. The PhAc-LKKR-AMC substrate was used in eight different concentrations (100, 50, 25, 10, 5, 2.5, 1.0, and 0 μ M; Supporting Information: Figure S6). IC_{50} -values and enzyme kinetic parameters were calculated from technical triplicates of each concentration (one dilution series of inhibitor, one batch of enzyme, and three wells containing the same reaction) using GRAFIT (Version 5.0.13; Erithacus Software Limited). K_i values for inhibitors were calculated from IC_{50} and the substrate K_M ($3.31 \pm 0.27 \mu$ M) using the Cheng-Prusoff equation.^[62]

4.4 | Isothermal titration calorimetry

ITC experiments in technical triplicates (at least 3 ITC experiments of the same inhibitor and enzyme batches, although several enzyme expressions and purifications were conducted to cover all experiments presented) were performed on a MicroCal PEAQ-ITC automated system (Malvern Instruments). Experiments were performed in assay buffer (20 mM TRIS [pH 8.5], 10% [v/v] Glycerol, 0.01% [v/v] Triton_{X-100}, 2 mM DTT) supplemented with 5% (v/v) DMSO to better match the conditions of the enzyme inhibition assay. 300–600 μ M of the ligands 1–3 was titrated to 15–20 μ M NS2B/NS3 if not stated elsewhere (Supporting Information: Figure S7). Since the K_d value for inhibitor 4 binding to NS2B/NS3 was too low to give a sufficient slope at the inflection point, a low- c titration^[63] was performed with a 20-fold molar excess of inhibitor 4 in the syringe resulting in 30–50 μ M NS2B/NS3 and 1–2 mM inhibitor 4 if not stated elsewhere (Supporting Information: Figure S7). For those measurements, the stoichiometry was set to 1.0. Control experiments (buffer vs. buffer, buffer vs. titrant, titrand vs. buffer) were subtracted from the raw data to correct offset. Experiments were performed at 25°C, the stirring speed was set to 750 rpm, and the reference power to 41.9 μ W. Nineteen injections $\pm 2 \mu$ l were added to the reaction cell with a duration of 4 s and a spacing time of 150 s. Data integration and evaluation were performed using the MicroCal PEAQ-ITC analysis software (Vers. 1.21, Malvern Panalytical Ltd). Corrections for the buffer ionization enthalpies resulting from proton transitions upon NS2B/NS3 binding were performed in assay buffer containing HEPES or BICINE instead of TRIS. Determination of changes in

isobaric heat capacity upon binding (ΔC_p) was performed in HEPES buffers at two additional temperatures (15°C and 35°C).

4.5 | MD simulations

MD simulations were performed starting from the ZIKV NS2B/NS3-1 complex structure (PDB-ID 6Y3B).^[27] An apo structure was generated by the removal of the ligand, while complexes with the ligands 2–4 were generated by manipulation (removal or addition of atoms) of the reference ligand 1 within the complex and subsequent energy minimization of the newly introduced ligand atoms within MOE^[64] using the Merck Molecular Force Field (MMFF94).^[65] The ligands were parameterized using the Generalized Amber Force Field (GAFF2^[66]) with AM1-BCC^[67] charges within antechamber^[68] of the AmberTools20.^[69] Complex structures were subsequently built with tleap^[69] including crystallographic solvent molecules. After initial relaxation over 200 time steps with sander, counter ions (Na⁺ for the protein–ligand complexes, Cl[−] for ligand simulations) were added and a TIP3P^[70] waterbox exceeding the structure by 10.0 Å was built with tleap. MDs were performed using NAMD2.14^[71] and the AMBER forcefield (ff14SB^[72]). The system was equilibrated over 1 ns by heating from 100 to 300 K over 500 ps and releasing harmonic constraints on the protein and ligand atoms over the following 500 ps in a constant volume box. MD production runs were performed over 10 ns with an NPT ensemble using periodic boundary conditions and a van der Waals cut-off of 14.0 Å with time steps of 2 fs allowing rigid bond lengths. For torsion energy analysis, ligand simulations without protein were conducted under the same conditions. Trajectories were written every ps and concatenated to include every 10th frame with catdcd 4.0 to result in 1000 frames per 10 ns prior analysis in VMD-1.9.3.^[73] Order parameters S^2 were calculated using the isotropic reorientational eigenmode dynamics (iRED) approach within cptraaj^[74] of the AmberTools20.^[69] Figures were created with PyMOL (The PyMOL Molecular Graphics System, Version 2.0 Schrödinger, LLC.).

4.6 | Crystallization and structure determination

The bZiPro/inhibitor complexes (molar ratio 1:12) were incubated for 1 h on ice at a protein concentration of 40 mg/ml. Two microliters of the bZiPro/inhibitor mixture was added to 2 μ l of the reservoir solution and incubated at 18°C in a hanging drop vapor diffusion experiment. The reservoir solution consisted of 0.1 M sodium acetate pH 4.6, 0.2 M ammonium sulfate, and 16%–19% PEG 2000. The PEG 2000 concentration was optimized separately for each inhibitor. Crystals appeared after 1 day and were cryoprotected using 30% PEG 2000 before being flash-frozen in liquid nitrogen. For inhibitor 2, macroseeding was performed to obtain sufficiently diffracting crystals. Crystals of bZiPro in complex with inhibitor 2 were transferred into a fresh drop consisting of 2 μ l

of the bZiPro/inhibitor mixture and 2 µl of the reservoir solution for 1 day. The new reservoir solution contained 2% less PEG 2000 compared to the initial reservoir solution.

Diffraction intensities were collected at BESSY MX beamline 14.1. Data processing and scaling were performed with the XDS program package.^[75] Structure determination was done by molecular replacement with PHASER MR using the bZiPro structure with the PDB code 5GPI as a model.^[76] Simulated annealing was performed within the initial refinement with PHENIX to remove potential bias from the search model.^[77,78] The structures were subjected to alternating rounds of manual rebuild using Coot^[79] to fit amino acids into σ -weighted $2F_o - F_c$ and $F_o - F_c$ electron density maps and the PHENIX refine program (five cycles). For the calculation of R_{free} , 5% of all data were randomly chosen and were not considered during refinement. Isotropic B-factor refinement with TLS parameters was used. Water and inhibitor molecules were located in the electron density and gradually added to the model. Multiple conformations were built if the minor populated conformation showed at least 20% occupancy. Coordinates and restraints for the inhibitors were generated with the Grade Web server.^[80] The structures were deposited in the Protein Data Bank with accession codes 7ZLD (2), 7ZLC (3), and 7ZMI (4). The final data collection and refinement statistics are summarized in Supporting Information: Table S7.

B-factors were normalized with the BANΔIT-webserver^[16] to analyze differences in protein binding-site flexibility in complex with the ligands 1–4 using the modified z-score method for C_α atoms of the protein backbone.

ACKNOWLEDGMENTS

The authors thank the Group of Prof. Dahai Luo for sharing the pETDuet-1 vector containing NS2B/NS3 (bZiPro) via Addgene (Watertown). They thank Anna Riede for excessive purifications of NS2B/NS3 and Prof. Dr. Tanja Schirmeister for access to facilities and instrumentation as well as scientific discussion on the project. The authors thank M. ed. Thomas Steinfurth for language proofreading of the manuscript. Parts of this research were conducted using the supercomputer Mogon and/or advisory services offered by Johannes Gutenberg University Mainz (hpc.uni-mainz.de), which is a member of the AHRP (Alliance for High Performance Computing in Rhineland Palatinate, www.ahrp.info) and the Gauss Alliance e.V. The authors gratefully acknowledge the computing time granted on the supercomputer Mogon at Johannes Gutenberg University Mainz (hpc.uni-mainz.de). The authors gratefully acknowledge the provision of synchrotron beamline at the Helmholtz-Zentrum Berlin (HZB, BL 14.1) and thank the scientific beamline staff at BESSY II for providing them with outstanding support during data collection. The authors thank the German Research Council (DFG) for supporting this work through the grant "DFG-Großgeräteeintrag ITC (INST 247/921-1 FUGG)." The authors are also grateful to Helmholtz-Zentrum Berlin (HZB) for financial support for travel costs. Torsten Steinmetzer obtained funding from the LOEWE Center DRUID (Novel Drug Targets against Poverty-Related and Neglected Tropical Infectious Diseases). Open Access funding enabled and organized by Projekt DEAL.

CONFLICT OF INTEREST

The authors declare no conflict of interest.

ORCID

Christian Kersten  <http://orcid.org/0000-0001-9976-7639>

REFERENCES

- [1] G. S. Campos, A. C. Bandeira, S. I. Sardi, *Emerg. Infect. Dis.* **2015**, *21*, 1885.
- [2] G. Kuno, *Mol. Detect. Hum. Viral Pathog.* **2016**, *503*, 313.
- [3] M. Hennessey, M. Fischer, J. E. Staples, *MMWR. Morb. Mortal. Wkly. Rep.* **2016**, *65*, 1.
- [4] A. N. Hazin, A. Poretti, D. Di Cavalcanti Souza Cruz, M. Tenorio, A. van der Linden, L. J. Pena, C. Brito, L. Gil, D. de Barros Miranda-Filho, E. Marques, C. M. Turchi Martelli, J. Alves, T. A. Huisman, *N. Engl. J. Med.* **2016**, *374*, 2193.
- [5] E. D'Ortenzio, S. Matheron, X. de Lamballerie, B. Hubert, G. Piorkowski, M. Maquart, D. Descamps, F. Damond, Y. Yazdanpanah, I. Leparc-Goffart, *N. Engl. J. Med.* **2016**, *374*, 2195.
- [6] J. F. W. Chan, G. K. Y. Choi, C. C. Y. Yip, V. C. C. Cheng, K. Y. Yuen, *J. Infect.* **2016**, *72*, 507.
- [7] J. Mlakar, M. Korva, N. Tul, M. Popović, M. Poljšak-Prijatelj, J. Mraz, M. Kolenc, K. Resman Rus, T. Vesnaver Vipotnik, V. Fabjan Vodusek, A. Vizjak, J. Pizem, M. Petrovec, T. Avšič Županc, *N. Engl. J. Med.* **2016**, *374*, 951.
- [8] M. R. Duffy, T.-H. Chen, W. T. Hancock, A. M. Powers, J. L. Kool, R. S. Lanciotti, M. Pretrick, M. Marfel, S. Holzbauer, C. Dubray, L. Guillaumot, A. Griggs, M. Bel, A. J. Lambert, J. Laven, O. Kosoy, A. Panella, B. J. Biggerstaff, M. Fischer, E. B. Hayes, *N. Engl. J. Med.* **2009**, *360*, 2536.
- [9] M. Aubry, A. Teissier, M. Huart, S. Merceron, J. Vanhomwegen, C. Roche, A.-L. Vial, S. Teururai, S. Sicard, S. Paulous, P. Desprès, J.-C. Manuguerra, H.-P. Mallet, D. Musso, X. Deparis, V.-M. Cao-Lormeau, *Emerg. Infect. Dis.* **2017**, *23*, 669.
- [10] V. M. Cao-Lormeau, A. Blake, S. Mons, S. Lastère, C. Roche, J. Vanhomwegen, T. Dub, L. Baudouin, A. Teissier, P. Larre, A. L. Vial, C. Decam, V. Choumet, S. K. Halstead, H. J. Willison, L. Musset, J. C. Manuguerra, P. Despres, E. Fournier, H. P. Mallet, D. Musso, A. Fontanet, J. Neil, F. Ghawché, *Lancet* **2016**, *387*, 1531.
- [11] B. D. Lindenbach, H.-J. Theil, C. M. Rice, *Fields Virol.* **2007**, *5*, 1101.
- [12] S. Voss, C. Nitsche, *Bioorg. Med. Chem. Lett.* **2020**, *30*, 126965.
- [13] É. E. da Silva Rodrigues, H. Maus, S. J. Hammerschmidt, A. Ruggieri, E. C. dos Santos, É. J. Bassi, L. Anderson, P. G. V. Aquino, J. X. de Araújo-Júnior, F. Wei, X. Liu, P. Zhan, T. Schirmeister, E. F. da Silva-Júnior, *Human Viruses: Diseases, Treatments and Vaccines* (Ed: S. I. Ahmad), Springer International Publishing, **2021**, 233.
- [14] B. Millies, F. Von Hammerstein, A. Gellert, S. Hammerschmidt, F. Barthels, U. Göppel, M. Immerheiser, F. Elgner, N. Jung, M. Basic, C. Kersten, W. Kiefer, J. Bodem, E. Hildt, M. Windbergs, U. A. Hellmich, T. Schirmeister, *J. Med. Chem.* **2019**, *62*, 11359.
- [15] H. Maus, F. Barthels, S. J. Hammerschmidt, K. Kopp, B. Millies, A. Gellert, A. Ruggieri, T. Schirmeister, *Bioorg. Med. Chem.* **2021**, *47*, 116392.
- [16] F. Barthels, T. Schirmeister, C. Kersten, *Mol. Inform.* **2021**, *40*, 1.
- [17] O. Carugo, *Acta Crystallogr. D Struct. Biol.* **2022**, *78*, 69.
- [18] A. Sandner, T. Hüfner-Wulsdorf, A. Heine, T. Steinmetzer, G. Klebe, *J. Med. Chem.* **2019**, *62*, 9753.
- [19] W. W. Phoo, Z. Zhang, M. Wirawan, E. J. C. Chew, A. B. L. Chew, J. Kouretova, T. Steinmetzer, D. Luo, *Antiviral Res.* **2018**, *160*, 17.
- [20] W. W. Phoo, Y. Li, Z. Zhang, M. Y. Lee, Y. R. Loh, Y. B. Tan, E. Y. Ng, J. Lescar, C. Kang, D. Luo, *Nat. Commun.* **2016**, *7*, 13410.

- [21] C. Götz, G. Hinze, A. Gellert, H. Maus, F. von Hammerstein, S. J. Hammerschmidt, L. M. Lauth, U. A. Hellmich, T. Schirmeister, T. Basché, *J. Phys. Chem. B* **2021**, *125*, 6837.
- [22] M. Brecher, Z. Li, B. Liu, J. Zhang, C. A. Koetzner, A. Alifarag, S. A. Jones, Q. Lin, L. D. Kramer, H. Li, *PLoS Pathog.* **2017**, *13*, e1006411.
- [23] M. E. Hill, M. Yildiz, J. A. Hardy, *Biochemistry* **2019**, *58*, 776.
- [24] P. Erbel, N. Schiering, A. D'Arcy, M. Renatus, M. Kroemer, S. P. Lim, Z. Yin, T. H. Keller, S. G. Vasudevan, U. Hommel, *Nat. Struct. Mol. Biol.* **2006**, *13*, 372.
- [25] E. F. da Silva-Júnior, J. X. de Araújo-Júnior, *Bioorg. Med. Chem.* **2019**, *27*, 3963.
- [26] S. Huber, N. J. Braun, L. C. Schmacke, J. P. Quek, R. Murra, D. Bender, E. Hildt, D. Luo, A. Heine, T. Steinmetzer, *J. Med. Chem.* **2022**, *65*, 6555.
- [27] N. J. Braun, J. P. Quek, S. Huber, J. Kouretova, D. Rogge, H. Lang-Henkel, E. Z. K. Cheong, B. L. A. Chew, A. Heine, D. Luo, T. Steinmetzer, *ChemMedChem* **2020**, *15*, 1439.
- [28] C. Nitsche, H. Onagi, J. P. Quek, G. Otting, D. Luo, T. Huber, *Org. Lett.* **2019**, *21*, 4709.
- [29] A. Poulsen, C. Kang, T. Keller, *Curr. Pharm. Des.* **2014**, *20*, 3422.
- [30] M. A. M. Behnam, D. Graf, R. Bartenschlager, D. P. Zlotos, C. D. Klein, *J. Med. Chem.* **2015**, *58*, 9354.
- [31] H. A. Lim, J. Joy, J. Hill, C. San Brian Chia, *Eur. J. Med. Chem.* **2011**, *46*, 3130.
- [32] M. J. Stoermer, K. J. Chappell, S. Liebscher, C. M. Jensen, C. H. Gan, P. K. Gupta, W. J. Xu, P. R. Young, D. P. Fairlie, *J. Med. Chem.* **2008**, *51*, 5714.
- [33] J. J. H. Chu, R. C. H. Lee, M. J. Y. Ang, W.-L. Wang, H. A. Lim, J. L. K. Wee, J. Joy, J. Hill, C. S. B. Chia, *Antiviral Res.* **2015**, *118*, 68.
- [34] H. M. Berman, *Nucleic Acids Res.* **2000**, *28*, 235.
- [35] M. Z. Hammamy, C. Haase, M. Hammami, R. Hilgenfeld, T. Steinmetzer, *ChemMedChem* **2013**, *8*, 231.
- [36] E. H. Rühmann, M. Rupp, M. Betz, A. Heine, G. Klebe, *ChemMedChem* **2016**, *11*, 309.
- [37] J. E. DeLorbe, J. H. Clements, M. G. Teresk, A. P. Benfield, H. R. Plake, L. E. Millspaugh, S. F. Martin, *J. Am. Chem. Soc.* **2009**, *131*, 16758.
- [38] A. P. Benfield, M. G. Teresk, H. R. Plake, J. E. DeLorbe, L. E. Millspaugh, S. F. Martin, *Angew. Chem. Int. Ed.* **2006**, *45*, 6830.
- [39] B. Wienen-Schmidt, H. R. A. Jonker, T. Wulsdorf, H. D. Gerber, K. Saxena, D. Kudlinzki, S. Sreeramulu, G. Parigi, C. Luchinat, A. Heine, H. Schwalbe, G. Klebe, *J. Med. Chem.* **2018**, *61*, 5922.
- [40] J. E. Delorbe, J. H. Clements, B. B. Whiddon, S. F. Martin, *ACS Med. Chem. Lett.* **2010**, *1*, 448.
- [41] B. P. Morgan, D. R. Holland, B. W. Matthews, P. A. Bartlett, *J. Am. Chem. Soc.* **1994**, *116*, 3251.
- [42] R. Derda, M. R. Jafari, *Prot. Pept. Lett.* **2019**, *25*, 1051.
- [43] G. Ruiz-Gómez, J. D. A. Tyndall, B. Pfeiffer, G. Abbenante, D. P. Fairlie, *Chem. Rev.* **2010**, *110*, PR1.
- [44] J. J. Li, D. D. Holsworth, L. Y. Hu, *Chemtracts* **2003**, *16*, 439.
- [45] J. R. Frost, C. C. G. Scully, A. K. Yudin, *Nat. Chem.* **2016**, *8*, 1105.
- [46] D. Yang, A. Singh, H. Wu, R. Kroe-Barrett, *Anal. Biochem.* **2016**, *508*, 78.
- [47] C. Velours, M. Aumont-Nicaise, S. Uebel, P. England, A. Velazquez-Campoy, D. Stroebel, G. Bec, P. Soule, C. Quéard, C. Ebel, A. Roussel, J. B. Charbonnier, P. F. Varela, *Eur. Biophys. J.* **2021**, *50*, 313.
- [48] A. Cooper, *Biophys. Chem.* **2005**, *115*, 89.
- [49] A. Velazquez-Campoy, N. Markova, *Malvern Panalytical: Knowledge Center* **2015**, *1*.
- [50] S. Vega, O. Abian, A. Velazquez-Campoy, *Biochim. Biophys. Acta.* **2016**, *1860*, 868.
- [51] G. A. Holdgate, A. Tunnicliffe, W. H. J. Ward, S. A. Weston, G. Rosenbrock, P. T. Barth, I. W. F. Taylor, R. A. Pauptit, D. Timms, *Biochemistry* **1997**, *36*, 9663.
- [52] E. Freire, J. Gómez, *J. Mol. Biol.* **1995**, *252*, 337.
- [53] A. Cooper, C. M. Johnson, J. H. Lakey, M. Nöllmann, *Biophys. Chem.* **2001**, *93*, 215.
- [54] A. Cooper, *J. Phys. Chem. Lett.* **2010**, *1*, 3298.
- [55] D. L. Cameron, J. Jakus, S. R. Pauleta, G. W. Pettigrew, A. Cooper, *J. Phys. Chem. B* **2010**, *114*, 16228.
- [56] G. Cui, J. M. Swails, E. S. Manas, *J. Chem. Theory Comput.* **2013**, *9*, 5539.
- [57] D. W. Li, R. Brüschweiler, *J. Am. Chem. Soc.* **2009**, *131*, 7226.
- [58] G. Lipari, A. Szabo, *J. Am. Chem. Soc.* **1982**, *104*, 4546.
- [59] H. Stöckmann, A. Bronowska, N. R. Syme, G. S. Thompson, A. P. Kalverda, S. L. Warriner, S. W. Homans, *J. Am. Chem. Soc.* **2008**, *130*, 12420.
- [60] J. D. Dunitz, *Chem. Biol.* **1995**, *2*, 709.
- [61] Z. Zhang, Y. Li, Y. R. Loh, W. W. Phoo, A. W. Hung, C. Kang, D. Luo, *Science* **2016**, *354*, 1597.
- [62] C. Yung-Chi, W. H. Prusoff, *Biochem. Pharmacol.* **1973**, *22*, 3099.
- [63] Y.-L. Zhang, Z.-Y. Zhang, *Anal. Biochem.* **1998**, *261*, 139.
- [64] I. Tubert-Brohman, W. Sherman, M. Repasky, T. Beuming, *J. Chem. Inf. Model.* **2013**, *53*, 1689.
- [65] T. a Halgren, *J. Comput. Chem.* **1996**, *17*, 490.
- [66] D. Vassetzki, M. Pagliai, P. Procacci, *J. Chem. Theory Comput.* **2019**, *15*, 1983.
- [67] A. Jakalian, D. B. Jack, C. I. Bayly, *J. Comput. Chem.* **2002**, *23*, 1623.
- [68] J. Wang, W. Wang, P. A. Kollman, D. A. Case, *J. Mol. Graph. Model.* **2006**, *25*, 247.
- [69] D. A. Case, T. E. Cheatham, T. Darden, H. Gohlke, R. Luo, K. M. Merz, A. Onufriev, C. Simmerling, B. Wang, R. J. Woods, *J. Comput. Chem.* **2005**, *26*, 1668.
- [70] W. L. Jorgensen, J. Chandrasekhar, J. D. Madura, R. W. Impey, M. L. Klein, *J. Chem. Phys.* **1983**, *79*, 926.
- [71] J. C. Phillips, R. Braun, W. Wang, J. Gumbart, E. Tajkhorshid, E. Villa, C. Chipot, R. D. Skeel, L. Kalé, K. Schulten, *J. Comput. Chem.* **2005**, *26*, 1781.
- [72] J. A. Maier, C. Martinez, K. Kasavajhala, L. Wickstrom, K. E. Hauser, C. Simmerling, *J. Chem. Theory Comput.* **2015**, *11*, 3696.
- [73] W. Humphrey, A. Dalke, K. Schulten, *J. Mol. Graphics* **1996**, *14*, 33.
- [74] D. R. Roe, T. E. Cheatham, *J. Chem. Theory Comput.* **2013**, *9*, 3084.
- [75] W. Kabsch, *Int. Tables Crystallogr.* **2006**, *F*, 218.
- [76] A. J. McCoy, *Acta Crystallogr. Sect. D Biol. Crystallogr.* **2006**, *63*, 32.
- [77] P. D. Adams, P. V. Afonine, G. Bunkóczi, V. B. Chen, I. W. Davis, N. Echols, J. J. Headd, L. W. Hung, G. J. Kapral, R. W. Grosse-Kunstleve, A. J. McCoy, N. W. Moriarty, R. Oeffner, R. J. Read, D. C. Richardson, J. S. Richardson, T. C. Terwilliger, P. H. Zwart, *Acta Crystallogr. D. Biol. Crystallogr.* **2010**, *66*, 213.
- [78] P. V. Afonine, R. W. Grosse-Kunstleve, N. Echols, J. J. Headd, N. W. Moriarty, M. Mustyakimov, T. C. Terwilliger, A. Urzhumtsev, P. H. Zwart, P. D. Adams, *Acta Crystallogr. D. Biol. Crystallogr.* **2012**, *68*, 352.
- [79] P. Emsley, K. Cowtan, *Acta Crystallogr. D. Biol. Crystallogr.* **2004**, *60*, 2126.
- [80] O. S. Smart, T. O. Womack, A. Sharff, C. Flensburg, P. Keller, W. Paciorek, C. Vonrhein, G. Bricogne, Cambridge, United Kingdom, Global Phasing Ltd. **2011**. <https://www.globalphasing.com>

SUPPORTING INFORMATION

Additional supporting information can be found online in the Supporting Information section at the end of this article.

How to cite this article: S. J. Hammerschmidt, S. Huber, N. J. Braun, M. Lander, T. Steinmetzer, C. Kersten, *Arch. Pharm.* **2023**;356:e2200518. <https://doi.org/10.1002/ardp.202200518>